

# The Relation between the Optical Fe II Emission and the Dimensionless Accretion Rate for Active Galactic Nuclei

YAN-SHENG LIU<sup>1</sup> AND WEI-HAO BIAN<sup>1</sup>

<sup>1</sup>*School of Physics and Technology, Nanjing Normal University, Nanjing 210023, China*

(Received XXXX XX, 2020)

## ABSTRACT

It was suggested that the prominent feature of the optical Fe II emission has a connection with the accretion process in active galactic nuclei (AGN). For a large sample of 4037 quasars ( $z < 0.8$ ) with measured  $H\beta$  line dispersion ( $\sigma_{H\beta}$ ) selected from the Sloan Digital Sky Survey (SDSS) and 120 compiled reverberation-mapped (RM) AGN, we use  $\sigma_{H\beta}$  and the extended  $R_{\text{BLR}}(H\beta) - L_{5100}$  relation to calculate supermassive black holes masses ( $M_{\text{BH}}$ ) from the single-epoch spectra for the SDSS subsample, and  $\sigma_{H\beta}$  from the mean spectra for the RM subsample. We find a strong correlation between the relative optical Fe II strength  $R_{\text{Fe}}$  and  $\mathcal{M}$  for the SDSS subsample with the Spearman correlation coefficient  $r_s$  of 0.727, which is consistent with that derived from the mean spectra for the RM subsample. The magnitude of velocity shift of the optical Fe II emission has a strong anticorrelation with  $\mathcal{M}$ , whenever there is inflow or outflow. These strong correlations show that the optical Fe II emission has an intimate connection with the accretion process. Assuming that the difference of  $M_{\text{BH}}$  is due to the variable virial factor  $f$  for adopting  $\text{FWHM}_{H\beta}$  as the velocity tracer, we find that there is a relation between  $f$  and  $\text{FWHM}_{H\beta}$ ,  $\log f = -(0.41 \pm 0.002) \log \text{FWHM}_{H\beta} + (1.719 \pm 0.009)$  for the single-epoch spectrum. The relation between  $\log f$  and  $\sigma_{H\beta}$  is not too strong, suggesting that  $\sigma_{H\beta}$  does not seem to depend much on the broad-line region inclination and a constant  $\sigma$ -based  $f$  is suitable for  $\sigma_{H\beta}$  as the velocity tracer.

*Keywords:* galaxies: active – galaxies: nuclei – galaxies: Seyfert – quasars: emission lines – quasars: general

## 1. INTRODUCTION

Fe II emissions shown in the optical and ultraviolet (UV) spectra are prominent features in most active galactic nuclei (AGN; e.g., Boroson & Green 1992; Hu et al. 2008; Shen & Ho 2014; Zhao et al. 2020). With the principal component analysis of a low- $z$  sample of 87 Palomar–Green quasars, Boroson & Green (1992) found that principal component 1 (PC1) is related to the relative strength of optical Fe II to the broad  $H\beta$  ( $R_{\text{Fe}}$ , the ratio between the strength of Fe II emission within 4434 – 4684 Å and the broad  $H\beta$ ), the FWHM of the broad  $H\beta$  ( $\text{FWHM}_{H\beta}$ ), [O III]5007 strength, and principal component 2 (PC2) links optical luminosity and  $\alpha_{\text{ox}}$  (optical-X-ray spectral index). PC1 and PC2 have relations with the accretion process around the supermassive black holes (SMBHs). With  $\text{FWHM}_{H\beta}$ -based SMBH masses ( $M_{\text{BH}}$ ), Boroson (2002) suggested that PC1 is mainly correlated with the Eddington ratio ( $L_{\text{Bol}}/L_{\text{Edd}}$ ,  $L_{\text{Bol}}$  is the bolometric luminosity and  $L_{\text{Edd}}$  is the Edding-

ton luminosity) and PC2 has a strong connection with  $M_{\text{BH}}$  and  $L_{\text{Bol}}/L_{\text{Edd}}$ . Using a large sample of the Sloan Digital Sky Survey (SDSS) quasars, Hu et al. (2008) did a detailed line-fitting technique and found the connections between the optical Fe II strength, velocity shift, and the Eddington ratio. Using a two-dimensional plane of  $\text{FWHM}_{H\beta}$  and  $R_{\text{Fe}}$  for the SDSS quasars, Shen & Ho (2014) suggested that the Eddington ratio is also a key factor to be considered in the orientation-based unification of quasar phenomenology (Urry & Padovani 1995).

In order to investigate the relation between Fe II features and the accretion process,  $M_{\text{BH}}$  is a key parameter needing to be determined. With effort over nearly two decades, the reverberation-mapping (RM) method with the  $H\beta$  spectral monitoring has been successfully applied for about 120 AGN (e.g., Blandford & McKee 1982; Peterson et al. 2004; Du et al. 2016a; Grier et al. 2017; Yu et al. 2020a,b; Hu et al. 2021). The RM method can measure the time lag between the line variation (e.g.,  $H\beta$ , Mg II, C IV) and the corresponding continuum variation, and give the broad-line region (BLR) distance from the central SMBH ( $R_{\text{BLR}}$ ). For type 1 AGN, the BLR clouds emitting the broad  $H\beta$  line can be used as a probe to calculate the virial mass (e.g.,

Peterson et al. 2004; Netzer 2013):

$$M_{\text{BH}} = f \times \frac{R_{\text{BLR}} (\Delta V)^2}{G}. \quad (1)$$

where  $\Delta V$  is the velocity of the BLR clouds,  $f$  is a corresponding virial factor, and  $G$  is the gravitational constant. Through the RM AGN, an empirical  $R_{\text{BLR}} - L_{5100}$  relation ( $L_{5100}$  is the 5100 Å monochromatic luminosity,  $R_{\text{BLR}} \propto L_{5100}^{0.5}$ ) was given and used to estimate  $R_{\text{BLR}}$  from a single-epoch spectrum (e.g., Kaspi et al. 2000; Bentz et al. 2013; Du et al. 2016b; Dalla Bontà et al. 2020; Khadka et al. 2022; Maithil et al. 2022). The changes of the spectral energy distribution, connected to changes in the accretion rate, would likely lead to the breadth (an increment in the scatter) in the empirical  $R_{\text{BLR}} - L_{5100}$  relation in the first-order consideration (Wang et al. 2014; Martínez-Aldama et al. 2019; Du & Wang 2019; Yu et al. 2020a; Maithil et al. 2022). AGN with strong Fe II emission show a smaller  $R_{\text{BLR}}$  than expected (e.g., Du & Wang 2019). Since  $R_{\text{Fe}}$  has a relation with the accretion rate (e.g., Netzer & Trakhtenbrot 2007; Du et al. 2016a; Yu et al. 2020a; Maithil et al. 2022), an extended  $R_{\text{BLR}}(\text{H}\beta) - L_{5100}$  relation ( $R_{\text{BLR}} \propto L_{5100}^{0.5} + R_{\text{Fe}}$ ) was recently suggested (Du & Wang 2019; Yu et al. 2020a; Khadka et al. 2022). The reduction in the scatter in the extended  $R_{\text{BLR}}(\text{H}\beta) - L_{5100}$  relation (Yu et al. 2020a) is in agreement with the one ( $\sim 0.13$  dex) previously reported by Kilerci Eser et al. (2015), who used the UV luminosity instead of  $L_{5100}$  as a substitute for the ionizing luminosity in the empirical  $R_{\text{BLR}}(\text{H}\beta) - L_{5100}$  relation. The extended  $R_{\text{BLR}}(\text{H}\beta) - L_{5100}$  relation would result in a better measurement of  $M_{\text{BH}}$ .

For the RM AGN,  $\Delta V$  is usually traced by four kinds of velocities, i.e., the broad  $\text{H}\beta$  FWHM or the line dispersion ( $\sigma_{\text{H}\beta}$ ) measured from the mean/rms spectrum (e.g., Peterson et al. 2004; Ho & Kim 2014; Yu et al. 2020b). From Equation 1,  $f = M_{\text{BH}}/(R_{\text{BLR}}(\Delta V)^2/G)$ . For four kinds of velocities  $\Delta V$ , the corresponding four kinds of virial factors  $f$  are defined, which are usually calibrated through the  $M_{\text{BH}} - \sigma_*$  relation ( $\sigma_*$  is the bulge stellar velocity dispersion) or other independent methods to derive the SMBH masses (e.g., Onken et al. 2004; Ho & Kim 2014; Yu et al. 2020b). For several multiple RM AGN, it was found  $\sigma_{\text{H}\beta}$  is better than  $\text{FWHM}_{\text{H}\beta}$  used to calculate  $M_{\text{BH}}$  with a constant factor  $f$  (Peterson et al. 2004). For the 120 RM AGN sample (Yu et al. 2020b), with respect to  $M_{\text{BH}}$  from  $\sigma_*$  or  $\sigma_{\text{H}\beta, \text{rms}}$ , it was found that we can obtain  $M_{\text{BH}}$  from  $\sigma_{\text{H}\beta, \text{mean}}$  with the smallest scatter than from  $\text{FWHM}_{\text{H}\beta}$ . Dalla Bontà et al. (2020) also suggested that the use of  $\sigma_{\text{H}\beta}$  gives better results, while the use of  $\text{FWHM}_{\text{H}\beta}$  introduces a bias, stretching the mass scale such that high masses are overestimated and low masses are underestimated, although both velocity tracers are usable. A variable FWHM-based  $f$  was suggested (Collin et al. 2006; Mejía-Restrepo et al. 2018; Yu et al.

2019, 2020b). The cumulative fraction of  $f$  was consistent with the a simple model of thick-diskBLRs, which implied that, as the tracer of BLRs velocity,  $\text{FWHM}_{\text{H}\beta}$  has some dependence on the BLRs inclination, while  $\sigma_{\text{H}\beta}$  is insensitive to the inclination (Collin et al. 2006; Yu et al. 2019). For AGN with the single-epoch spectrum,  $\text{FWHM}_{\text{H}\beta}$  or  $\sigma_{\text{H}\beta}$  is used to trace  $\Delta V$ , which was used in large surveys, such as SDSS (Shen et al. 2011). With respect to the  $\text{H}\beta$  FWHM,  $\sigma_{\text{H}\beta}$  was preferred to calculate  $M_{\text{BH}}$  from the single-epoch spectrum (Yu et al. 2020b). With Equation 1,  $M_{\text{BH}} = f_\sigma \times \sigma_{\text{H}\beta}^2 R_{\text{BLR}}(\text{H}\beta)/G = f_{\text{FWHM}} \times \text{FWHM}_{\text{H}\beta}^2 R_{\text{BLR}}(\text{H}\beta)/G$ . Considering a variable  $f_{\text{FWHM}}$  in  $\text{FWHM}_{\text{H}\beta}$ -based  $M_{\text{BH}}$ , it means

$$f_{\text{FWHM}} = f_\sigma (\sigma_{\text{H}\beta}/\text{FWHM}_{\text{H}\beta})^2. \quad (2)$$

About the accretion strength, there are mainly two parameters, the Eddington ratio  $L_{\text{Bol}}/L_{\text{Edd}}$  and the dimensionless accretion rate  $\dot{\mathcal{M}}$ , where  $\dot{\mathcal{M}} \equiv \dot{M}/\dot{M}_{\text{Edd}}$ ,  $\dot{M}_{\text{Edd}} = L_{\text{Edd}}/c^2$ . The accretion rate  $\dot{M}$  can be derived from the disk model of Shakura & Sunyaev (1973), which has been extensively applied to fit the spectra of AGN (e.g., Collin et al. 2002; Bian & Zhao 2003; Davis & Laor 2011; Mejía-Restrepo et al. 2018). Considering that the radius  $R$  distribution of the effective disk temperature is given by  $T_{\text{eff}} \propto R^{-3/4}$ ,  $\dot{\mathcal{M}}$  is (e.g., Du et al. 2016a)

$$\dot{\mathcal{M}} \equiv \dot{M}/\dot{M}_{\text{Edd}} = 20.1 \left( \frac{l_{44}}{\cos i} \right)^{3/2} m_7^{-2}. \quad (3)$$

where  $l_{44} = L_{5100}/10^{44} \text{erg s}^{-1}$ ,  $m_7 = M_{\text{BH}}/10^7 M_\odot$ . An average value of  $\cos i = 0.75$  is adopted, which corresponds to the opening angle of the dusty torus (e.g., Davis & Laor 2011; Du et al. 2016a).  $\dot{\mathcal{M}}$  is inversely proportional to  $M_{\text{BH}}$  to the second power. This Equation applies to AGN that have  $\log(\dot{\mathcal{M}}/M_\odot)$  between -2 and 3.5, namely excluding the regimes of advection-dominated accretion flows ( $\log(\dot{\mathcal{M}}/M_\odot) < -2$ ) and of flows with hyper-accretion rates ( $\log(\dot{\mathcal{M}}/M_\odot) > 3.5$ ). Using FWHM-based  $M_{\text{BH}}$  and  $L_{\text{Bol}}/L_{\text{Edd}}$  for 63 RM AGN, Du et al. (2016a) found  $R_{\text{Fe}}$  correlated with  $L_{\text{Bol}}/L_{\text{Edd}}$  and  $\dot{\mathcal{M}}$  (also see Netzer & Trakhtenbrot 2007; Hu et al. 2008; Maithil et al. 2022). They also suggested the BLRs "fundamental plane", i.e., a strong bivariate correlation of  $\dot{\mathcal{M}}$  with  $R_{\text{Fe}}$  and the  $\text{H}\beta$  shape  $\text{FWHM}_{\text{H}\beta}/\sigma_{\text{H}\beta}$ .

In this paper, we use a large sample of 4037 SDSS quasars ( $z < 0.8$ ; Hu et al. 2008) with measured broad  $\text{H}\beta$  line dispersion  $\sigma_{\text{H}\beta}$  and  $R_{\text{Fe}}$  to investigate again the relation between Fe II emission and the accretion process, as well as a subsample of 120 RM AGN. About the accretion strength, we use  $\dot{\mathcal{M}}$  instead of  $L_{\text{Bol}}/L_{\text{Edd}}$ . We also derive the relation between  $f_{\text{FWHM}}$  and  $\text{FWHM}_{\text{H}\beta}$  for the single-epoch spectrum. This paper is organized as follows. Section 2 presents

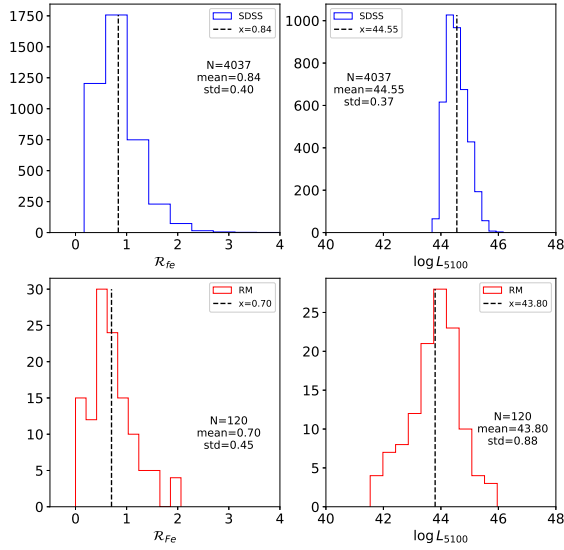


**Figure 1.** Distributions of  $R_{\text{Fe}}$  and  $L_{5100}$  for the subsample of 4037 SDSS quasars (top panels, blue) and the subsample of 120 RM AGN (bottom panels, red). The dashed lines are their mean values. The number, the mean value, and the standard deviation are shown in panels.

the adopted samples and data analysis. Section 3 is our results and discussions. Section 4 is our conclusions. All of the cosmological calculations in this paper assume  $\Omega_{\Lambda} = 0.7$ ,  $\Omega_{\text{M}} = 0.3$ , and  $H_0 = 70 \text{ km s}^{-1} \text{ Mpc}^{-1}$ .

## 2. SAMPLES AND DATA ANALYSIS

Because we use  $\sigma_{\text{H}\beta}$  instead of  $\text{FWHM}_{\text{H}\beta}$  to calculate  $M_{\text{BH}}$ , the spectral decomposition is crucial. We use a subsample of 4037 quasars ( $z < 0.8$ ) from SDSS presented by Hu et al. (2008) with criteria of signal-to-noise ratio ( $\text{S/N}$ )  $> 10$  and  $\text{EW}(\text{Fe II}) > 25 \text{ \AA}$ . We briefly introduce their spectral fitting (Hu et al. 2008). The continuum is decomposed into three components: a single power law, Balmer continuum emission, and a pseudocontinuum due to blended Fe II emission. For the pure emission-line spectrum subtracting the continuum, the narrow  $\text{H}\beta$  component, [O III]4959, 5007 are modeled using Gaussians, and the broad  $\text{H}\beta$  component is modeled using a Gauss-Hermite function, whose best fit yields the  $\text{FWHM}_{\text{H}\beta}$ ,  $\sigma_{\text{H}\beta}$ . At the same time, we also use a compiled subsample of 120 RM AGN with measured four kinds of velocity tracers from mean and rms spectra (Yu et al. 2020b, and references therein). About the 120 RM subsample (Yu et al. 2020a), we mainly adopted the data from Du et al. (2016a) and Shen et al. (2019). For 63 AGN in this RM subsample, Du et al. (2016a) used the same fitting scheme as Hu et al. (2008). They included the host correction in the fitting described in Hu et al. (2015). For other

44 SDSS AGN in the RM subsample, Shen et al. (2019) used almost the same fitting scheme as Hu et al. (2015). For this subsample of 120 RM AGN, the flux of broad optical Fe II is all measured by integration from 4434 to 4684  $\text{\AA}$ ,  $z$  is less than 1.026, host-corrected  $L_{5100}$  is between  $10^{41.54}$  and  $10^{45.95} \text{ erg s}^{-1}$ . In order to use all of available RM AGN, no criterion on  $\text{EW}(\text{Fe II})$  or  $\text{S/N}$  is used.

For the SDSS subsample,  $L_{5100}$ , the Fe II luminosity, the broad  $\text{H}\beta$  luminosity,  $\text{FWHM}_{\text{H}\beta}$  and  $\sigma_{\text{H}\beta}$  are adopted, respectively, from columns (15), (3), (9), (11), (41) in Table 2 in Hu et al. (2008). The ratio of the luminosity of Fe II to the broad  $\text{H}\beta$  is calculated as  $R_{\text{Fe}}$  with its error calculated from the error transfer formula. With respect to [O III]  $\lambda 5007$ , the Fe II velocity shift and its error are adopted from columns (7)-(8) in Table 2 in Hu et al. (2008). For the RM subsample,  $L_{5100}$  and  $R_{\text{Fe}}$  are adopted from columns (3) and (7) in Table 1 in Yu et al. (2020a), as well as their errors. Using the relative variance fraction  $F_{\text{var}}$ , Hu et al. (2015) gave Fe II RM for 10 narrow-line Seyfert 1 galaxies (NLS1s). They found that all 10 objects show Fe II variations with an amplitude of a few to 10%. On average, the variability of Fe II is about 10% smaller than the variability of the  $\text{H}\beta$  line. As the variability of  $\text{H}\beta$  is unusually much larger than that of Fe II, the uncertainties of  $R_{\text{Fe}}$  are mainly governed by  $\text{H}\beta$  variability, which on average is  $\sim 20\%$  (Hu et al. 2015; Du et al. 2016a).  $\text{FWHM}_{\text{mean}}$ ,  $\sigma_{\text{H}\beta, \text{mean}}$ ,  $\text{FWHM}_{\text{rms}}$ ,  $\sigma_{\text{H}\beta, \text{rms}}$  and their errors are adopted from columns (4)-(7) in Table 1 in Yu et al. (2020b).

In Figure 1, we show the distributions of  $L_{5100}$  and  $R_{\text{Fe}}$  for the SDSS subsample and the RM subsample. It is clear that the RM subsample has averagely smaller  $L_{5100}$  than the SDSS subsample. We perform the Kolmogorov–Smirnov (K–S) test<sup>1</sup> on distributions in Figure 1. The statistic  $d$  and the significant level probability for the null hypothesis ( $p$ -value) are -0.18 and 0.0001 for  $R_{\text{Fe}}$ , 0.52 and  $2.22 \times 10^{-16}$  for  $L_{5100}$ , respectively. The distribution of  $R_{\text{Fe}}$  has a difference between the two subsamples and the difference of the  $L_{5100}$  distribution is more significant. In Figure 2, we show the distributions of  $\text{FWHM}_{\text{H}\beta}$ ,  $\sigma_{\text{H}\beta}$ , and the broad  $\text{H}\beta$  shape  $D_{\text{H}\beta, \text{mean}} \equiv \text{FWHM}_{\text{H}\beta} / \sigma_{\text{H}\beta}$  from the mean spectrum for the RM subsample (red lines). It was found that  $D_{\text{H}\beta, \text{mean}}$  has a relation with  $L_{\text{Bol}} / L_{\text{Edd}}$  or  $\mathcal{M}$  (e.g., Collin et al. 2006; Du et al. 2016a; Yu et al. 2020a; Panda 2022). We also show the distribution of  $\text{FWHM}_{\text{H}\beta}$  and  $\sigma_{\text{H}\beta}$  from the single-epoch spectrum for the SDSS subsample (blue lines). We perform the K–S test on distributions in Figure 2 and find no significant differences between the two samples. The statistic  $d$  and  $p$ -value for the null hy-

<sup>1</sup> We used python (scipy.stats.ks\_2samp, scipy.stats.spearmanr) to do our following analysis for the K-S test and the Spearman correlation test.

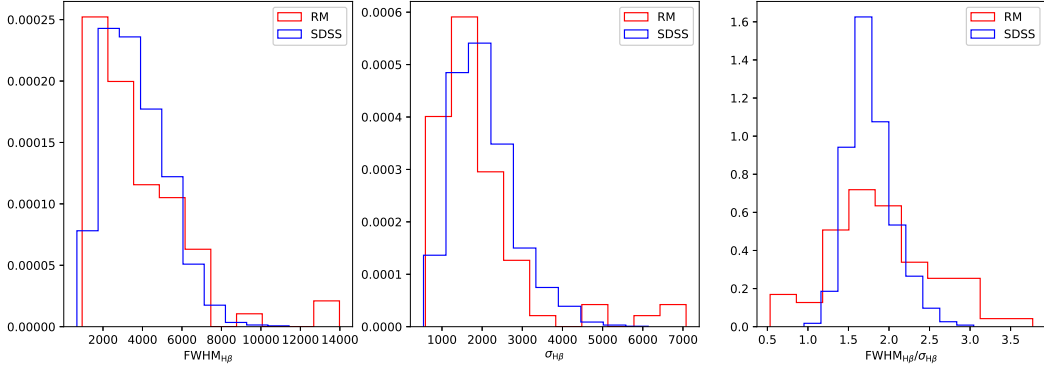


**Figure 2.** Distributions of  $\text{FWHM}_{\text{H}\beta}$ ,  $\sigma_{\text{H}\beta}$ , and their ratio  $\text{FWHM}_{\text{H}\beta}/\sigma_{\text{H}\beta}$  for the broad  $\text{H}\beta$ . The blue lines are for the subsample of 4037 SDSS quasars. The red lines are for the subsample of 120 RM AGN. The fractional numbers are used to compare the distributions for two subsamples.

pothesis are 0.17 and 0.03 for  $\text{FWHM}_{\text{H}\beta}$ , 0.20 and 0.005 for  $\sigma_{\text{H}\beta}$ , 0.24 and 0.0004 for  $\text{FWHM}_{\text{H}\beta}/\sigma_{\text{H}\beta}$ , respectively. The value of  $\text{FWHM}_{\text{H}\beta}/\sigma_{\text{H}\beta}$  is 2.35, 3.46, 2.45, 2.83, and 0 for a Gaussian, a rectangular, a triangular, an edge-on rotating ring, and a Lorentzian profile, respectively (Collin et al. 2006; Du et al. 2016a). For the SDSS subsample, the mean value and its standard deviation for  $\text{FWHM}_{\text{H}\beta}/\sigma_{\text{H}\beta}$  are 1.78 and 0.28 (see right panel in Figure 2). For the RM subsamples, the mean value and its standard deviation are 1.94 and 0.61. They show the deviation from the value of 2.35 for the single Gaussian profile. There are 37 NLS1s with  $\text{FWHM}_{\text{H}\beta} < 2000 \text{ km s}^{-1}$  from the mean spectrum for the RM subsample and 564 NLS1s from the single-epoch spectrum for the SDSS subsample (e.g., Bian & Zhao 2004). With respect to the proportion of the number of NLS1s in the SDSS subsample ( $\sim 14\%$ ), the higher proportion in the RM subsample ( $\sim 31\%$ ) is due to including an RM project searching for super-Eddington accreting massive black holes (SEAMBHs; Wang et al. 2013; Du et al. 2016a). The mean and its standard deviation of  $D_{\text{H}\beta, \text{mean}}$  for NLS1s are 1.53 and 0.27 for the RM subsample, 1.50 and 0.15 for the SDSS subsample, which are much deviated from the value of 2.35 for the single Gaussian profile.

For the SDSS subsample,  $L_{5100}$  is from  $\sim 10^{44}$  to  $\sim 10^{46} \text{ erg s}^{-1}$ , the mean value and the standard deviation of  $\log L_{5100}$  are 44.55 and 0.37. We use the empirical formula to correct the host contribution (Shen et al. 2011; Ge et al. 2016),

$$\frac{L_{5100, \text{host}}}{L_{5100, \text{QSO}}} = 0.8052 - 1.5502x + 0.9121x^2 - 0.1577x^3. \quad (4)$$

for  $x + 44 \equiv \log(L_{5100, \text{total}}/\text{erg s}^{-1}) < 45.053$ . There are 3590/4037 AGN with luminosities below this value, and no correction is needed for luminosities above this value. For host-corrected  $\log(L_{5100}/\text{erg s}^{-1})$ , the mean value is 44.40,

which is smaller than uncorrected mean values of 44.55 by 0.15 dex.

### 3. RESULTS AND DISCUSSIONS

#### 3.1. $M_{\text{BH}}$ , $\mathcal{M}$ and $L_{\text{Bol}}/L_{\text{Edd}}$

An extended empirical  $R_{\text{BLR}}(\text{H}\beta) - L_{5100}$  relation including  $R_{\text{Fe}}$  was found for the RM AGN subsample (Du & Wang 2019; Yu et al. 2020a):

$$\log \frac{R_{\text{BLR}}(\text{H}\beta)}{l_{44}} = (0.48 \pm 0.03) \log l_{44} - (0.38 \pm 0.04) R_{\text{Fe}} + (1.67 \pm 0.09) \quad (5)$$

For  $\log R_{\text{BLR}}(\text{H}\beta)$ , it has an intrinsic scatter of 0.17 dex (Yu et al. 2020a). We adopt a systematic error of 0.2 dex in our following calculation. With the extended  $R_{\text{BLR}}(\text{H}\beta) - L_{5100}$  relation, when  $\sigma_{\text{H}\beta}$  is used as the tracer of the virial velocity, and  $f$  is adopted as 5.5 (e.g., Yu et al. 2020a,b), the single-epoch virial mass formula can be expressed as

$$\log \frac{M_{\text{BH}, \sigma_{\text{H}\beta}}}{M_{\odot}} = 7.7 + 2 \log \frac{\sigma_{\text{H}\beta}}{1000 \text{ km s}^{-1}} + (0.48 \pm 0.03) \log l_{44} - (0.38 \pm 0.04) R_{\text{Fe}} \quad (6)$$

When we use  $\text{FWHM}_{\text{H}\beta}$  as the tracer of the virial velocity, and adopt  $f$  as 1 (e.g., Du & Wang 2019), the single-epoch virial mass formula can be expressed as

$$\log \frac{M_{\text{BH}, \text{FWHM}_{\text{H}\beta}}}{M_{\odot}} = 6.96 + 2 \log \frac{\text{FWHM}_{\text{H}\beta}}{1000 \text{ km s}^{-1}} + (0.48 \pm 0.03) \log l_{44} - (0.38 \pm 0.04) R_{\text{Fe}} \quad (7)$$

Substitute Equation 6 for Equation 3, the  $\mathcal{M}$  formula is:

$$\log(\mathcal{M}_{\sigma_{\text{H}\beta}}) = (0.54 \pm 0.06) \log l_{44} - 4 \log \frac{\sigma_{\text{H}\beta}}{1000 \text{ km s}^{-1}} + (0.76 \pm 0.08) R_{\text{Fe}} + 0.09 \quad (8)$$

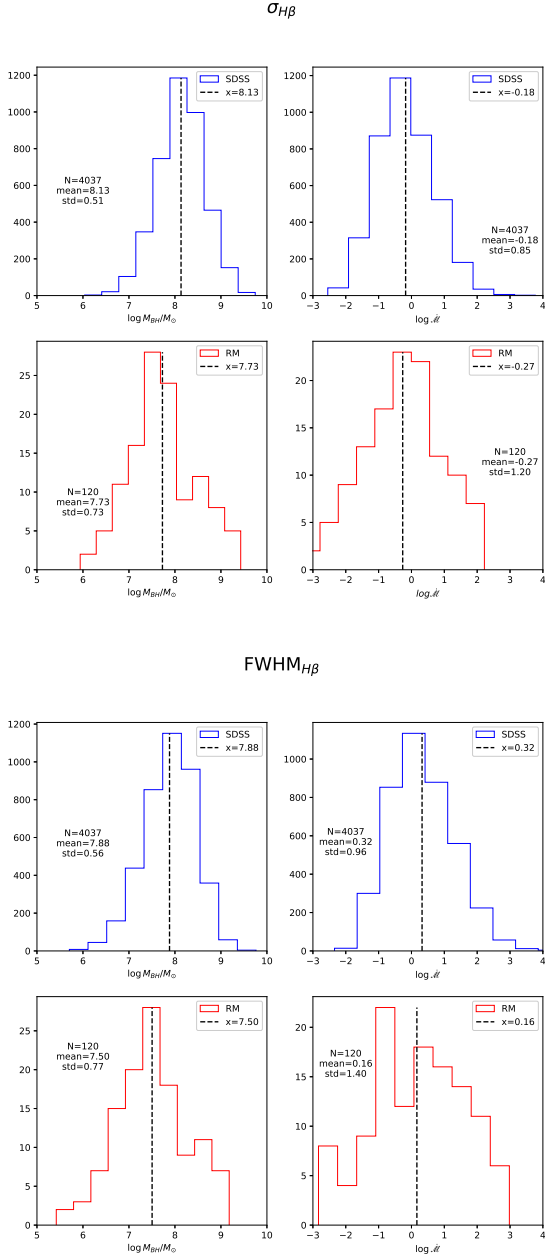


**Figure 3.** Distributions for  $M_{\text{BH}}$  and  $\dot{M}$  derived from  $\sigma_{H\beta}$  (top two panels) and  $\text{FWHM}_{H\beta}$  (bottom two panels) for the subsample of 4037 SDSS quasars (blue) and the subsample of 120 RM AGN (red). The dashed lines are mean values. The number, the mean value, and the standard deviation are shown in panels.

When using  $\text{FWHM}_{H\beta}$ , a similar  $\dot{M}$  formula is:

$$\log(\dot{M}_{\text{FWHM}_{H\beta}}) = (0.54 \pm 0.06) \log l_{44} - 4 \log \frac{\text{FWHM}_{H\beta}}{1000 \text{ km s}^{-1}} + (0.76 \pm 0.08) R_{\text{Fe}} + 1.57 \quad (9)$$

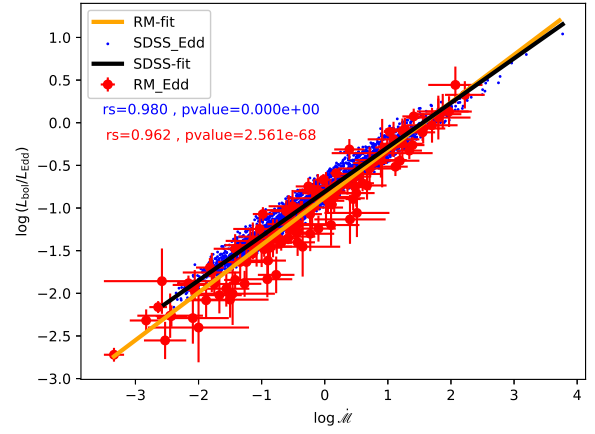


**Figure 4.**  $L_{\text{Bol}}/L_{\text{Edd}}$  versus  $\dot{M}$  for the subsample of 4037 SDSS quasars (blue points) and the subsample of 120 RM AGN (red points). The black and orange solid lines are the best linear fittings for the SDSS subsample and the RM subsample.

We use a correction factor to calculate  $L_{\text{Bol}}$  from  $L_{5100}$ ,  $L_{\text{Bol}} = BC_{5100} L_{5100}$ , where  $BC_{5100} = 53 - \log(L_{5100}/\text{erg s}^{-1})$  (Marconi et al. 2004; Netzer 2013). In the following sections, if not stated,  $\text{FWHM}_{H\beta}$  and  $\sigma_{H\beta}$  are from the mean spectrum for the RM subsample, and we will adopt the  $\sigma_{H\beta}$ -based  $M_{\text{BH}}$  and  $\dot{M}$  from the single-epoch spectrum for the SDSS subsample and from the mean spectrum for the RM subsample.

For the SDSS subsample of 4037 AGN, using  $\sigma_{H\beta}$  or  $\text{FWHM}_{H\beta}$  from the single-epoch spectrum and the extended  $R_{\text{BLR}}(H\beta) - L_{5100}$  relation, from Equations 6 or 7, we calculate  $M_{\text{BH}}$ . Based on the error transfer formula, the error of  $M_{\text{BH}}$  is calculated from the errors of  $\sigma_{H\beta}$  or  $\text{FWHM}_{H\beta}$ ,  $L_{5100}$ ,  $R_{\text{Fe}}$ , including a systematic error of 0.2 dex for  $R_{\text{BLR}}(H\beta)$ . For the RM subsample of 120 RM AGN, using  $\sigma_{H\beta}$  or  $\text{FWHM}_{H\beta}$  from the mean spectrum and  $R_{\text{BLR}}(H\beta)$  measured through RM technique, from Equation 1,  $M_{\text{BH}}$  was presented in Yu et al. (2020b), as well as its error. We use Equation 3 to calculate  $\dot{M}$ , as well as its error. In Figure 3, we show the distributions of  $M_{\text{BH}}$  (left panels) and  $\dot{M}$  (right panels) for the SDSS subsample and the RM subsample. Left two top panels show the mean value and the standard deviation of  $\log M_{\text{BH}}$  from  $\sigma_{H\beta}$  are 8.13 and 0.51 for the SDSS subsample; 7.73 and 0.73 for the RM subsample. The former is averagely larger than the latter by 0.4 dex. It is mainly due to a large  $L_{5100}$  for the SDSS subsample. The left two bottom panels show that for  $M_{\text{BH}}$  calculated from  $\text{FWHM}_{H\beta}$ . For the SDSS subsample, the mean values of  $\sigma_{H\beta}$ -based  $M_{\text{BH}}$  and  $\text{FWHM}_{H\beta}$ -based  $M_{\text{BH}}$  are 8.13 and 7.88. For the RM subsample, the mean values of  $\sigma_{H\beta}$ -based  $M_{\text{BH}}$  and  $\text{FWHM}_{H\beta}$ -based  $M_{\text{BH}}$  are 7.73 and 7.5. The  $\sigma_{H\beta}$ -based  $M_{\text{BH}}$  is averagely larger than  $\text{FWHM}_{H\beta}$ -based

$M_{\text{BH}}$  for the SDSS subsample (by 0.25 dex) or the RM subsample (by 0.23 dex). It is smaller than 0.5 dex found in [Bian et al. \(2008\)](#). The right two top panels show  $\dot{M}$  calculated from  $\sigma_{\text{H}\beta}$ . Right two bottom panels shows that for  $\dot{M}$  calculate from  $\text{FWHM}_{\text{H}\beta}$ . The  $\sigma_{\text{H}\beta}$ -based  $\dot{M}$  is averagely smaller than  $\text{FWHM}_{\text{H}\beta}$ -based  $\dot{M}$  for the SDSS subsample (by 0.5 dex) or the RM subsample (by 0.43 dex). We perform the K-S tests on the distributions in Figure 3 between the SDSS subsample and the RM subsample. For  $\sigma_{\text{H}\beta}$ -based  $M_{\text{BH}}$ ,  $d = 0.344$ ,  $p\text{-value} = 8.60 \times 10^{-13}$ ; for  $\sigma_{\text{H}\beta}$ -based  $\dot{M}$ ,  $d = 0.123$ ,  $p\text{-value} = 0.053$ ; for  $\text{FWHM}_{\text{H}\beta}$ -based  $M_{\text{BH}}$ ,  $d = 0.320$ ,  $p\text{-value} = 4.29 \times 10^{-11}$ ; for  $\text{FWHM}_{\text{H}\beta}$ -based  $\dot{M}$ ,  $d = 0.165$ ,  $p\text{-value} = 0.0031$ . The difference of  $\dot{M}$  for these two subsamples is not significant while the  $M_{\text{BH}}$  difference for these two subsamples is significant.

A criterion of  $\dot{M} \geq 3$  is adopted to select super-Eddington accreting massive black holes (e.g., [Wang et al. 2013](#); [Du et al. 2016a](#)). Using  $\sigma_{\text{H}\beta}$ -based  $\dot{M}$ , there are 912/4037 super-Eddington accreting AGN in the SDSS subsample, and 40/120 super-Eddington accreting AGN in the RM subsample. A relative large proportion of super-Eddington accreting AGN in the SDSS subsample is due to the criterion of  $\text{EW}(\text{FeII}) > 25\text{\AA}$ . For the RM subsample, there are 25 AGN presented by the SEAMBH collaboration ([Wang et al. 2013](#); [Du et al. 2016a](#)).

In Figure 4, we show the  $L_{\text{Bol}}/L_{\text{Edd}}$  and  $\dot{M}$  for the SDSS subsample (blue dots) or the RM subsample (red dots). For the SDSS subsample, considering the errors in both coordinates, the best linear fitting through `kmpfit`<sup>2</sup> is  $\log L_{\text{Bol}}/L_{\text{Edd}} = -(0.808 \pm 0.001) + (0.521 \pm 0.002) \log \dot{M}$ . For the RM subsample, the best linear fitting is  $\log L_{\text{Bol}}/L_{\text{Edd}} = -(0.876 \pm 0.013) + (0.558 \pm 0.013) \log \dot{M}$ . The latter relation is steeper than the former. The slope difference is due to the larger  $L_{5100}$  for the SDSS subsample (see Figure 1). It is consistent with the result by [Maithil et al. \(2022\)](#) (see their Figure 6). These slopes are consistent with the slopes of 0.53 found by [Davis & Laor \(2011\)](#) and 0.52 by [Huang et al. \(2020\)](#). Using Equations 1 and 3,  $\dot{M} \propto L_{5100}^{1.5} M_{\text{BH}}^{-2}$ ,  $L_{\text{Bol}}/L_{\text{Edd}} \propto L_{\text{Bol}} M_{\text{BH}}^{-1} \propto L_{5100} M_{\text{BH}}^{-1}$ , so  $L_{\text{Bol}}/L_{\text{Edd}} \propto \dot{M}^{0.5} L_{5100}^{0.25}$ . The dependence on  $L_{5100}$  is smaller than on  $\dot{M}$ . The slope of 0.5 is well consistent with our slope of 0.52 or 0.56. The nonlinear relation between  $L_{\text{Bol}}/L_{\text{Edd}}$  and  $\dot{M}$  (although it is linear when the values of the logarithm are considered) would have an impact on the relations using  $\dot{M}$  instead of  $L_{\text{Bol}}/L_{\text{Edd}}$ . Considering  $L_{\text{Bol}} = \eta \dot{M} c^2$ , where  $\eta$  is the accretion efficiency,  $L_{\text{Bol}}/L_{\text{Edd}} = \frac{\eta \dot{M} c^2}{M_{\text{Edd}} c^2} = \eta \dot{M}$ .

Adopting  $L_{\text{Bol}}/L_{\text{Edd}} \propto \dot{M}^{0.5} L_{5100}^{0.25}$ , it means that  $\eta \propto \dot{M}^{-0.5} L_{5100}^{0.25} \propto (L_{\text{Bol}}/L_{\text{Edd}})^{-1} L_{5100}^{0.5}$ . The nonlinear relation implies that the converting efficiency  $\eta$  is anticorrelated with  $\dot{M}$  or  $L_{\text{Bol}}/L_{\text{Edd}}$  (including a relatively weaker dependence on  $L_{5100}$ ), i.e., smaller efficiency with higher dimensionless accretion rate.

### 3.2. $R_{\text{Fe}}$ versus $\dot{M}$

In Figure 5, we show the relation between  $R_{\text{Fe}}$  and  $\dot{M}$ . For the RM subsample, the Spearman correlation test gives a strong correlation with the coefficient  $r_s = 0.423$  and the probability of the null hypothesis  $p_{\text{null}} = 1.48 \times 10^{-6}$ . Considering the errors in both coordinates, the `kmpfit` fitting gives  $R_{\text{Fe}} = (0.713 \pm 0.047) + (0.532 \pm 0.066) \log \dot{M}$ . Excluding 44 SDSS RM AGN from the subsample of 120 RM AGN, the correlation is stronger with  $r_s = 0.60$ ,  $p_{\text{null}} = 9.3 \times 10^{-9}$ . Considering the errors in both coordinates, the fitting gives  $R_{\text{Fe}} = (0.548 \pm 0.053) + (0.564 \pm 0.074) \log \dot{M}$ . Considering errors, these slopes are consistent. For the SDSS subsample, the correlation is strong with  $r_s = 0.727$ ,  $p_{\text{null}} = 0$ . Considering the errors in both coordinates, the best linear fitting through `kmpfit` gives  $R_{\text{Fe}} = -(0.936 \pm 0.006) + (0.600 \pm 0.008) \log \dot{M}$ . There exists some difference in intercepts for the SDSS subsample and the RM subsample. The slightly intercept difference implies that  $\sigma_{\text{H}\beta}$ -based  $M_{\text{BH}}$  for the SDSS subsample is slightly overestimated leading to an underestimated in  $\dot{M}$ . For 44 SDSS RM AGN from the RM subsample, the correlation between  $R_{\text{Fe}}$  and  $\dot{M}$  is very weak with  $r_s = 0.06$ ,  $p_{\text{null}} = 0.686$ . This weak correlation is possibly due to the large uncertainties in the RM measurement of  $R_{\text{BLR}}$  for SDSS-RM AGN. Excluding these 44 SDSS RM AGN from the RM subsample, for the relation between  $R_{\text{Fe}}$  and  $\dot{M}$ ,  $r_s$  increases from 0.423 to 0.60, and  $p_{\text{null}}$  decreases from  $1.48 \times 10^{-6}$  to  $9.3 \times 10^{-9}$ . Considering the errors in both coordinates, for these 44 SDSS RM AGN from the RM subsample, the `kmpfit` fitting gives  $R_{\text{Fe}} = (0.661 \pm 0.072) + (0.466 \pm 0.115) \log \dot{M}$ . Although with a large scatter, its slope of 0.466 is flatter than for the fitting relation for the SDSS subsample (0.6) and the total RM subsample (0.532). The underestimation of  $\dot{M}$  is smaller than for the SDSS subsample. We recognize that the much larger correlation coefficient ( $r_s = 0.727$  for the SDSS subsample) is in part an effect of self-correlation induced by  $R_{\text{Fe}}$  in the extended R-L relationship to estimate  $M_{\text{BH}}$  and  $\dot{M}$ . Including  $R_{\text{Fe}}$  to calculate  $\dot{M}$ , the distribution of the SDSS subsample is well consistent with that for the RM subsample (see left panel in Figure 5).

We investigate this correlation for super-Eddington and sub-Eddington AGN (see Table 1). For 912 super-Eddington AGN in the SDSS subsample ( $\dot{M} > 3$ ; e.g., [Du et al. 2016a](#)),  $r_s = 0.57$  and  $p_{\text{null}} = 2.35 \times 10^{-79}$ . For 3125 sub-Eddington AGN in the SDSS subsample,  $r_s = 0.56$  and

<sup>2</sup> <https://www.astro.rug.nl/software/kapteyn/kmpfittutorial.html>. `kmpfit` is the Kapteyn Package Python binding for a piece of software that provides a robust and relatively fast way to perform nonlinear least-squares curve and surface fitting.

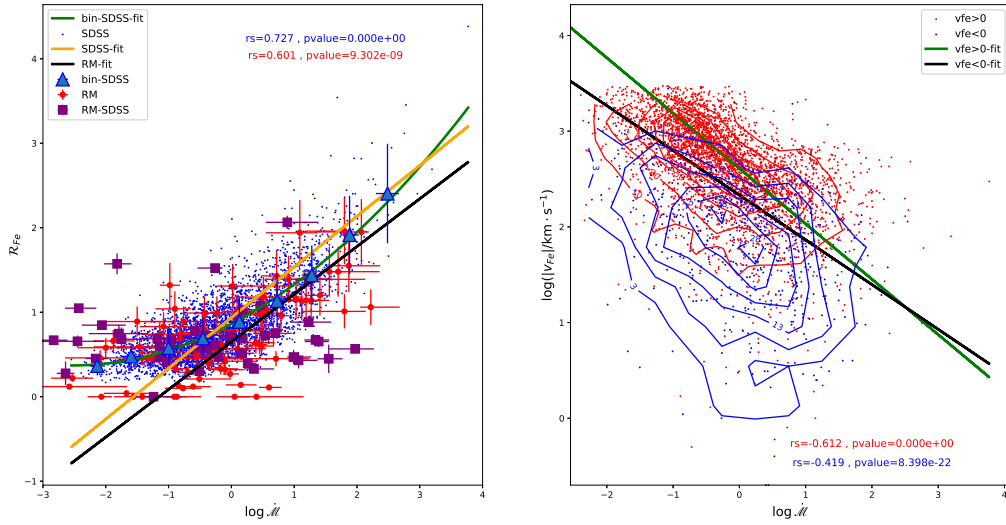


**Figure 5.** Left:  $R_{\text{Fe}}$  versus  $\dot{M}$ . The green line and black line are the best linear fittings for the SDSS subsample (blue points) and the RM subsample (red points). The blue triangles represent the mean  $R_{\text{Fe}}$  in bins of  $\Delta \log \dot{M} = 0.6$  dex, and the error bars represent the standard deviations. The green solid line shows the best fit to the binned data with a second-order polynomial function. The purple squares denote 44 RM SDSS AGN from the RM subsample. The  $r_s$  and  $p_{\text{null}}$  for the RM subsample are the ones excluding the SDSS RM AGN. Right:  $v_{\text{Fe}}$  versus  $\dot{M}$  for the SDSS subsample. The green line and black line are the best linear fittings for the inflow AGN ( $v_{\text{Fe}} > 0$ , red points and red contours) and the outflow AGN ( $v_{\text{Fe}} < 0$ , blue points and blue contours).

$p_{\text{null}} = 3.45 \times 10^{-252}$ . For super-Eddington accreting AGN, the slope is steeper than for sub-Eddington accretion AGN. For the RM subsample, for 40 super-Eddington RM AGN,  $r_s = 0.43$  and  $p_{\text{null}} = 0.0052$ . For 80 sub-Eddington RM AGN,  $r_s = 0.1$  and  $p_{\text{null}} = 0.38$ , which shows the correlation is not significant.

The systematic uncertainty is about 0.3 dex in  $M_{\text{BH}}$ , 0.6 dex in  $\dot{M}$  (e.g., Yu et al. 2020b). For the relation between  $R_{\text{Fe}}$  and  $\dot{M}$ , using  $\Delta \log \dot{M} = 0.6$  dex as the bin width, we calculate the mean and the standard deviation as the error in each bin. It shows a steeper slope with increasing  $\dot{M}$ . Using 2th-order polynomial function, we find the best fitting is  $R_{\text{Fe}} = (0.863 \pm 0.024) + (0.389 \pm 0.014) \log \dot{M} + (0.077 \pm 0.009)(\log \dot{M})^2$ , which can be used to estimate  $\dot{M}$  from  $R_{\text{Fe}}$  (Du et al. 2016a).

For a slightly smaller RM sample of 63 AGN (Du et al. 2016a), using FWHM-based  $\dot{M}$ , it was found that  $R_{\text{Fe}} = (0.66 \pm 0.04) + (0.30 \pm 0.03) \log \dot{M}$  ( $r_s = 0.65$ ). For 9818 SDSS DR4 AGN, it was found that, using FWHM-based  $M_{\text{BH}}$ , there was a correlation between  $R_{\text{Fe}}$  and  $L_{\text{Bol}}/L_{\text{Edd}}$  shown in Figure 5 of Netzer & Trakhtenbrot (2007),  $R_{\text{Fe}} \propto (L_{\text{Bol}}/L_{\text{Edd}})^{0.7}$ . Considering the nonlinear relation between  $L_{\text{Bol}}/L_{\text{Edd}}$  and  $\dot{M}$ ,  $L_{\text{Bol}}/L_{\text{Edd}} \propto \dot{M}^{0.52}$ , it implied  $R_{\text{Fe}} \propto \dot{M}^{0.36}$  for 9818 AGN by Netzer & Trakhtenbrot (2007), which is consistent with the result by Du et al. (2016a). These slopes are flatter than ours, which is due to larger  $M_{\text{BH}}$  and smaller  $\dot{M}$  using  $\sigma_{\text{H}\beta}$  instead of  $\sigma_{\text{H}\beta}$ . The strong cor-

relation between  $R_{\text{Fe}}$  and  $\dot{M}$  or  $L_{\text{Bol}}/L_{\text{Edd}}$  show that the relative strength of optical Fe II is driven by the strength of the accretion process. We also can use  $R_{\text{Fe}}$  to trace  $\dot{M}$  or  $L_{\text{Bol}}/L_{\text{Edd}}$  though with a large scatter. Including the  $\text{H}\beta$  shape  $\text{FWHM}_{\text{H}\beta}/\sigma_{\text{H}\beta}$ , for the SDSS subsample, the  $r_s$  increases from 0.727 to 0.75. For the RM subsample, the  $r_s$  increases from 0.423 to 0.46;  $p_{\text{null}}$  decreases from  $1.48 \times 10^{-6}$  to  $1.12 \times 10^{-7}$ . It is found that, including  $\text{FWHM}_{\text{H}\beta}/\sigma_{\text{H}\beta}$ , we cannot improve significantly the relation between  $\dot{M}$  and  $R_{\text{Fe}}$  (see also Du et al. 2016a).

### 3.3. $v_{\text{Fe}}$ versus $\dot{M}$

For the SDSS subsample of 4037 AGN, a systematic redshift of optical Fe II relative to  $[\text{O III}]\lambda 5007$  ( $v_{\text{Fe}}$ ) was found by Hu et al. (2008). The errors of  $v_{\text{Fe}}$  were calculated from the fitting of the continuum and the fitting of the  $[\text{O III}]\lambda 5007$  line, which was consistent with that given by the simulations. The median of the  $v_{\text{Fe}}$  distribution is  $116 \text{ km s}^{-1}$  (Hu et al. 2008). Sulentic et al. (2012) called into question the measurement of  $v_{\text{Fe}}$  in Hu et al. (2008). The contradictory results are possibly due to the different ways to construct their composite spectra. Sulentic et al. (2012) constructed them from bins by parameters of their 4D Eigenvector 1 (EV1) formalism, namely,  $\text{H}\beta$  FWHM and  $R_{\text{Fe}}$ , while Hu et al. (2008) constructed them from bins in  $v_{\text{Fe}}$ . Hu et al. (2012) confirmed that the redshift measurements of Fe II are robust.

**Table 1.** The Spearman correlation coefficient and the probability of the null hypothesis for relations.

	SDSS Subsample			RM Subsample		
	All	$\dot{M} < 3$	$\dot{M} \geq 3$	All	$\dot{M} < 3$	$\dot{M} \geq 3$
Number	4037	3125	912	120	80	40
$R_{\text{Fe}} - \dot{M}$	(0.727, 0)	(0.56, $3.45 \times 10^{-252}$ )	(0.57, $2.35 \times 10^{-79}$ )	(0.423, $1.48 \times 10^{-6}$ )	(0.1, 0.38)	(0.43, 0.0052)
$v_{\text{Fe}} - \dot{M}^*$	(-0.612, 0)*	(0.52, $2.37 \times 10^{-190}$ )*	(-0.08, 0.02)	-	-	-
$L_{\text{Bol}}/L_{\text{Edd}} - \dot{M}$	(0.98, 0)	-	-	(0.962, $2.56 \times 10^{-68}$ )	-	-

Note: The first value in brackets is the Spearman correlation coefficient and the second value is the probability of the null hypothesis.

\*: For the 3556 AGN with Fe II inflow ( $v_{\text{Fe}} > 0$ ) in the SDSS subsample with 2809 sub-Eddington ( $\dot{M} < 3$ ) and 747 super-Eddington ( $\dot{M} \geq 3$ ).

For the SDSS subsample of 4037 AGN, it is found there is a relation between  $v_{\text{Fe}}$  and  $\text{FWHM}_{\text{FeII}}$  with  $r_s = 0.59$ ,  $p_{\text{null}} = 0$ . For the relation between  $v_{\text{Fe}}$  and  $\text{FWHM}_{\text{H}\beta}$ ,  $r_s = 0.50$ ,  $p_{\text{null}} = 9.51 \times 10^{-229}$  (also see Figure 9 in Hu et al. 2008). It was found that the Eddington ratio is the main physical driver for  $v_{\text{Fe}}$  (Hu et al. 2008). In the right panel in Figure 5, for the SDSS subsample of 4037 AGN, we show the relation between  $v_{\text{Fe}}$  and  $\dot{M}$ . The correlations are strong with  $r_s = -0.612$ ,  $p_{\text{null}} = 0$  for 3556 AGN with Fe II inflow ( $v_{\text{Fe}} > 0$ ), and  $r_s = -0.419$ ,  $p_{\text{null}} = 9.40 \times 10^{-22}$  for 480 AGN with Fe II outflow ( $v_{\text{Fe}} < 0$ ), respectively. Considering the errors in both coordinates, the kmpfit fitting shows that  $\log v_{\text{Fe}} = (2.610 \pm 0.007) + (-0.578 \pm 0.01) \log \dot{M}$  for  $v_{\text{Fe}} > 0$  (green line in right panel in Figure 5). It is  $\log |v_{\text{Fe}}| = (2.331 \pm 0.018) + (-0.467 \pm 0.022) \log \dot{M}$  for  $v_{\text{Fe}} < 0$  (black line). For 3556 AGN with Fe II inflow ( $v_{\text{Fe}} > 0$ ) in the SDSS subsample, there are 2809 sub-Eddington AGN ( $\dot{M} < 3$ ),  $r_s = -0.52$  and  $p_{\text{null}} = 2.37 \times 10^{-190}$ . For 747 super-Eddington AGN with Fe II inflow ( $v_{\text{Fe}} > 0$ ),  $r_s = -0.08$ , and  $p_{\text{null}} = 0.02$ , which shows the correlation is not significant (see Table 1).

Using  $\sigma_{\text{H}\beta}$  and  $R_{\text{BLR}}(\text{H}\beta) \propto L_{5100}^{0.69}$  (McGill et al. 2008), for Fe II inflow ( $v_{\text{Fe}} > 0$ ), it was found that  $\log v_{\text{Fe}} = (1.00 \pm 0.05) + (-1.83 \pm 0.05) \log L_{\text{Bol}}/L_{\text{Edd}}$ ,  $r_s = -0.53$ ,  $p_{\text{null}} < 1.0 \times 10^{-5}$  (Hu et al. 2008). Considering the nonlinear relation between  $L_{\text{Bol}}/L_{\text{Edd}}$  and  $\dot{M}$ ,  $L_{\text{Bol}}/L_{\text{Edd}} \propto \dot{M}^{0.52}$ , it implied  $v_{\text{Fe}} \propto \dot{M}^{-0.95}$ . Here using  $\sigma_{\text{H}\beta}$ , the extended  $R_{\text{BLR}}(\text{H}\beta) - L_{5100}$  relation including  $R_{\text{Fe}}$  and the host-corrected  $L_{5100}$  to calculate  $M_{\text{BH}}$ , and the standard accretion disk to calculate  $\dot{M}$ , we find that the slope is  $-0.578 \pm 0.01$ . The flatter relation is due to the smaller  $R_{\text{BLR}}(\text{H}\beta)$  for larger  $R_{\text{Fe}}$ , which leads to smaller  $M_{\text{BH}}$  and larger  $\dot{M}$ . For the relation between  $v_{\text{Fe}}$  and  $\dot{M}$  shown in right panel in Fig. 5, excluding extreme accretors with  $\log \dot{M}$  larger than 1.5, we found that the correlation does not improve. It becomes slightly weaker with  $r_s$  changing from 0.612 to 0.602. For Fe II outflow ( $v_{\text{Fe}} < 0$ ), we also find a flatter relation with a slope of  $-0.467 \pm 0.022$  (see the black line in the right panel in Figure 5). It suggests that the inflow velocity is slightly larger than the outflow velocity for AGN with the same  $\dot{M}$ . The velocity of Fe II is driven by gravity toward the center and decelerated by the radiation

pressure, as well as its initial velocity. The redward shift of Fe II and the inverse correlation between  $v_{\text{Fe}}$  and  $\dot{M}$  favor a scenario in which Fe II emission emerges from an inflow (Hu et al. 2008). An increase in  $\dot{M}$  would enhance the radiation pressure and lead to a decrease of the inward velocity of the inflow.

From the general form of the equation of motion for a cloud of mass  $M_c$ , the acceleration  $a(r) = a_{\text{rad}}(r) - g(r) - \frac{1}{\rho} \frac{dP}{dr} + f_d/M_c$  (Netzer 2013), where  $g(r)$  is the gravitational acceleration,  $a_{\text{rad}}(r)$  is the acceleration due to radiation pressure force, and  $f_d$  is the drag force;  $P$  is the thermal pressure [ $P = \rho v_s^2$ , where  $v_s = (2k_B T / \mu m_{\text{H}})^{1/2} \sim 16.6(T/10^4 \text{K})^{1/2} \text{km s}^{-1}$ ,  $\mu m_{\text{H}}$  is the average mass per particle, and  $\mu = 0.6$ ]. Neglecting the gas pressure gradient and the drag force for pure wind flows,  $a(r) = a_{\text{rad}}(r) - g(r) \approx \frac{\sigma_{\text{r}} L}{4\pi r^2 \mu m_{\text{H}} c} [M(r) - \frac{L_{\text{Edd}}}{L}] = \frac{G}{r^2} M_{\text{BH}} [M(r) \frac{L}{L_{\text{Edd}}} - 1]$ .  $L$  is the total luminosity, and approximately equals  $L_{\text{Bol}}$ .  $M(r)$  is force multiplier, which is the ratio of the total radiation pressure to the radiation pressure due to Compton scattering.  $M(r) \geq 1$ , and  $M(r) = 1$  for fully ionized gas. Assuming the Fe II clouds falls down from torus (at  $r_1$ ) with an initial  $v_0 = 0$  to Fe II region at  $r_2$  ( $\sim R_{\text{BLR}}(\text{H}\beta)$ ), for the cases of constant  $[M(r) \frac{L}{L_{\text{Edd}}} - 1]$ , we get  $v^2 = 2GM_{\text{BH}}(1 - M \frac{L}{L_{\text{Edd}}})(\frac{1}{r_2} - \frac{1}{r_1})$ . Assuming the size of the innermost part of the torus is  $r_1 = nr_2$ , where  $n \sim 3 - 4$  (Netzer 2013), and  $M_{\text{BH}} = f \text{FWHM}_{\text{H}\beta}^2 \Gamma_2 / G$ , we get  $v_{\text{Fe}}^2 \approx 2 \frac{n-1}{n} f \text{FWHM}_{\text{H}\beta}^2 (1 - M(r) \frac{L}{L_{\text{Edd}}})$ . The force multiplier  $M(r)$  was found to be inversely correlated with the ionization parameter (Chelouche & Netzer 2005). Assuming  $M(r) = M_0 (L/L_{\text{Edd}})^{-\alpha}$ , we get  $v_{\text{Fe}}^2 \approx 2 \frac{n-1}{n} f \text{FWHM}_{\text{H}\beta}^2 [1 - M_0 (L/L_{\text{Edd}})^{1-\alpha}]$ . A smaller  $v$  would be found for AGN with larger  $L_{\text{Bol}}/L_{\text{Edd}}$ , and smaller  $\text{FWHM}_{\text{H}\beta}$  (also see Figure 9 in Hu et al. 2008).

However, we find that it is not the case for the blueward shift of Fe II, i.e., a smaller velocity of Fe II outflow for larger  $\dot{M}$ . The reason for the relation between the blueward velocity  $v_{\text{Fe}}$  and  $\dot{M}$  is not clear.

#### 3.4. The relation between $f$ and $\text{FWHM}_{\text{H}\beta}$

Assuming a variable  $f$  in  $\text{FWHM}_{\text{H}\beta}$ -based  $M_{\text{BH}}$  for the single-epoch or the mean spectrum, from Equation 2,  $\log f = 2 \log(\sigma_{\text{H}\beta}/\text{FWHM}_{\text{H}\beta}) + \log f_{\sigma}$ . In the left panel in Fig-



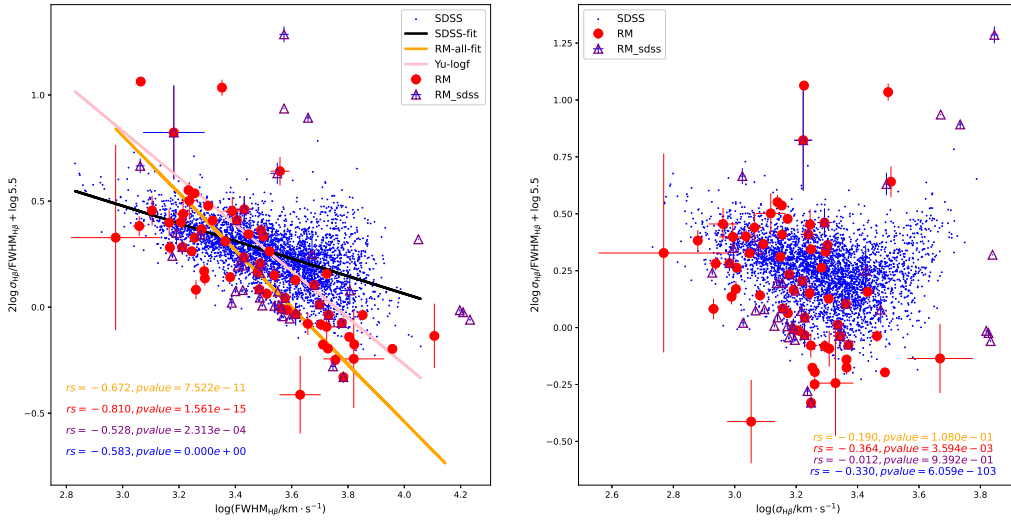


**Figure 6.** Left:  $f_{\text{FWHM}}$  versus  $\text{FWHM}_{\text{H}\beta}$ . The black line and orange line are the best linear fittings for the SDSS subsample (blue points) and the RM subsample (red points and triangles). The triangles show 44 RM AGN from the SDSS. The red points show other 76 compiled RM AGN excluding 44 RM AGN from the SDSS. The pink line is the relation given by Yu et al. (2020b). Right:  $f_{\text{FWHM}}$  versus  $\sigma_{\text{H}\beta}$  for the subsample of 120 RM AGN from the mean spectrum. The symbols are the same as in the left panel. The Spearman correlation coefficient and the probability of the null hypothesis are shown in panels. The blue is for the SDSS Subsample, the purple is for 44 RM AGN from the SDSS; the red is for the RM subsample excluding 44 RM AGN from the SDSS; the orange is for the RM subsample.

ure 6, we show  $\log f$  versus  $\text{FWHM}_{\text{H}\beta}$  where  $f_{\sigma} = 5.5$  as suggested by Yu et al. (2020b). For the SDSS subsample (blue points), the correlation is strong with  $r_s = -0.583$ ,  $p_{\text{null}} = 0$ . Considering the errors in both coordinates, the best fitting is  $\log f = (1.719 \pm 0.028) - (0.414 \pm 0.008) \log \text{FWHM}_{\text{H}\beta}$  (black line in the left panel in Figure 6) for the single-epoch spectrum. For  $\text{FWHM}_{\text{H}\beta} = 1000 \text{ km s}^{-1}, 2000 \text{ km s}^{-1}, 6000 \text{ km s}^{-1}, 14196 \text{ km s}^{-1}$ ,  $f = 3, 2.25, 1.42, 1$ , respectively. For the SDSS subsample, assuming the same  $M_{\text{BH}}$  from  $\text{FWHM}_{\text{H}\beta}$ ,  $\sigma_{\text{H}\beta}$  and  $f_{\sigma} = 5.5$ , the flatter slope means  $f$  has a narrow range, i.e., from 3 to 1 for  $\text{FWHM}_{\text{H}\beta}$  from 1000 to 14196  $\text{km s}^{-1}$ . For the value of 2.35 for the single Gaussian profile,  $\log f = 2 \log(\sigma_{\text{H}\beta} / \text{FWHM}_{\text{H}\beta}) + \log f_{\sigma} = 0.0017$ . The relation between  $\log f$  and  $\text{FWHM}_{\text{H}\beta}$  also shows the relation between  $\text{FWHM}_{\text{H}\beta} / \sigma_{\text{H}\beta}$  and  $\text{FWHM}_{\text{H}\beta}$ ,  $\log \text{FWHM}_{\text{H}\beta} / \sigma_{\text{H}\beta} = -0.49 + 0.207 \log \text{FWHM}_{\text{H}\beta}$ . In the left panel in Figure 6, almost all of the AGN with  $\text{FWHM}_{\text{H}\beta} < 4000 \text{ km s}^{-1}$  (Population A, Marziani et al. 2001) in the SDSS subsample show  $\text{FWHM}_{\text{H}\beta} / \sigma_{\text{H}\beta} < 2.35$  deviated from that for the single Gaussian H $\beta$  profile.

For the RM subsample, the Spearman correlation test gives  $r_s = -0.672$ ,  $p_{\text{null}} = 7.522 \times 10^{-11}$ . Considering the errors in both coordinates, the best-fitting relation for RM subsample shows  $\log f = -(1.348 \pm 0.080) \log \text{FWHM}_{\text{H}\beta} + (4.851 \pm 0.27)$  (orange solid line in Figure 6). Excluding 44 RM AGN from SDSS, the correlation is stronger with

$r_s = -0.81$ ,  $p_{\text{null}} = 1.5 \times 10^{-15}$ . The best-fitting relation is  $\log f = -(1.357 \pm 0.069) \log \text{FWHM}_{\text{H}\beta} + (4.883 \pm 0.232)$ . For 17 RM AGN with measured  $\sigma_*$  (Yu et al. 2020b), it was found that the relation is  $\log f = -(1.10 \pm 0.4) \log \text{FWHM}_{\text{H}\beta} + (4.13 \pm 0.11)$  (pink solid line in the left panel in Figure 6). Although our fitting slope for the RM subsample is steeper than Yu et al. (2020b), the trend is similar, i.e., larger  $f$  for AGN with smaller  $\text{FWHM}_{\text{H}\beta}$ . With our large number of AGN, the error of our slope is smaller, and our slope is consistent with the slope from RM AGN measured  $\sigma_*$  (Yu et al. 2020b) considering their large error. For the SDSS subsample, the slope derived from the single-epoch spectrum is flatter with respect to that for the RM subsample from the mean spectrum, i.e.,  $-0.414$  vs.  $-1.348$ .

Using  $\sigma_{\text{H}\beta, \text{rms}}$  as the benchmark instead of  $\sigma_{\text{H}\beta, \text{mean}}$  in Equation 2, for 120 RM AGN,  $r_s = -0.482$ ,  $p_{\text{null}} = 9.18 \times 10^{-4}$ . Considering the errors in both coordinates, the best-fitting relation is  $\log f = -(1.418 \pm 0.266) \log \text{FWHM}_{\text{H}\beta} + (5.148 \pm 0.08)$ . Excluding 44 RM AGN from SDSS, the correlation is stronger with  $r_s = -0.616$ ,  $p_{\text{null}} = 1.01 \times 10^{-7}$ . Considering the errors in both coordinates, the best-fitting relation is  $\log f = -(1.05 \pm 0.40) \log \text{FWHM}_{\text{H}\beta} + (3.755 \pm 0.40)$ . Considering their errors, these slopes are consistent with that using  $\sigma_{\text{H}\beta, \text{mean}}$  as the benchmark. A smaller  $\sigma_{\text{H}\beta}$ -based  $f_{\sigma}$  was suggested to be  $4.47_{-1.08}^{+1.41}$  for the single-epoch spectrum (Woo et al. 2015), or  $4.31 \pm 1.05$  (Grier et al. 2013) for the rms spectrum. Adopting these smaller  $f$ , it

would lead our best fitting of the relation between  $f$  and  $\text{FWHM}_{\text{H}\beta}$  to have a smaller intercept by  $\sim 0.1$  dex.

Because there is a strong relation between  $\dot{M}$  and  $\text{FWHM}_{\text{H}\beta}$  (e.g., [Bian & Zhao 2003](#)), it implies that, using  $\text{FWHM}_{\text{H}\beta}$  as a velocity tracer in the  $M_{\text{BH}}$  calculation, the corresponding  $f$  has a correlation with  $\dot{M}$ , i.e., a larger  $f$  is needed for AGN with larger  $\dot{M}$ . For a simple model of thick-disk BLRs, neglecting the contribution of outflow in the H $\beta$  profile, we obtained  $f = 1/(a^2 + \sin^2\theta)$ , where  $a$  is the ratio of the scale height of the thick disk to the radius  $r$ , and  $\theta$  is the inclination of the thick-disk of BLRs to the line of sight ([Collin et al. 2006](#); [Yu et al. 2019](#)). The cumulative fraction of this variable  $f$  for 34 RM AGN with measured stellar velocity dispersion  $\sigma_*$  was consistent with this simple model of thick-disk BLRs ([Yu et al. 2019](#)). The relation between  $f$  and  $\text{FWHM}_{\text{H}\beta}$  implied that, as the tracer of BLRs velocity,  $\text{FWHM}_{\text{H}\beta}$  has some dependence on the BLRs inclination, while  $\sigma_{\text{H}\beta}$  is insensitive to the inclination ([Collin et al. 2006](#); [Yu et al. 2019](#)).

In right panel in Figure 6, we show  $\log f$  versus  $\sigma_{\text{H}\beta}$  for the RM subsample (red points and triangles) and for the SDSS subsample (blue points). The Spearman correlation test gives  $r_s = -0.190$ ,  $p_{\text{null}} = 1.08 \times 10^{-1}$  for the RM subsample, which is not too significant. Excluding 44 RM AGN from SDSS, the correlation is always not strong with  $r_s = -0.364$ ,  $p_{\text{null}} = 3.59 \times 10^{-3}$ . Only for 44 RM AGN from SDSS, the correlation is very weak with  $r_s = -0.012$ ,  $p_{\text{null}} = 9.392 \times 10^{-1}$ . For the SDSS subsample,  $r_s = -0.33$ ,  $p_{\text{null}} = 6.06 \times 10^{-103}$ , which is weaker than that with  $\text{FWHM}_{\text{H}\beta}$ . Using  $\sigma_{\text{H}\beta, \text{rms}}$  as the benchmark instead of  $\sigma_{\text{H}\beta, \text{mean}}$  in Equation 2 (see the right panel in Figure 6), the Spearman correlation test gives  $r_s = -0.084$ ,  $p_{\text{null}} = 5.88 \times 10^{-1}$  for the RM subsample, which is not too significant. Excluding 44 RM AGN from SDSS, the correlation is always not strong with  $r_s = -0.249$ ,  $p_{\text{null}} = 5.09 \times 10^{-2}$ . If assuming the virial factor  $f$  has a dependence on the BLR inclination to the line of sight, these not significant correlations in the right panel show that  $\sigma_{\text{H}\beta}$  has no dependence on the inclination. It is consistent with the constant  $f$  using  $\sigma_{\text{H}\beta}$  as the velocity tracer in the  $M_{\text{BH}}$  calculation.

#### 4. CONCLUSIONS

For a large sample of 4037 SDSS quasars ( $z < 0.8$ ) with measured  $\sigma_{\text{H}\beta}$  and  $R_{\text{Fe}}$  and 120 compiled RM AGN, we use  $\sigma_{\text{H}\beta}$  instead of  $\text{FWHM}_{\text{H}\beta}$  and the extended  $R_{\text{BLR}}(\text{H}\beta) - L_{5100}$  relation (including  $R_{\text{Fe}}$ ) to calculate  $M_{\text{BH}}$  from the single-epoch spectra for the SDSS subsample, and  $\sigma_{\text{H}\beta}$  from the mean spectra for the RM subsample. We use  $\dot{M}$  instead of  $L_{\text{Bol}}/L_{\text{Edd}}$  to indicate the accretion strength to investigate the relation with optical Fe II emission ( $R_{\text{Fe}}$  and  $v_{\text{Fe}}$ ). We also derive the relation between the virial factor  $f$  and

$\text{FWHM}_{\text{H}\beta}$  for the single-epoch spectrum. The main conclusions can be summarized as follows:

- For the subsample of 4037 SDSS quasars, with respect to  $\text{FWHM}_{\text{H}\beta}$ ,  $\sigma_{\text{H}\beta}$ -based  $M_{\text{BH}}$  are averagely larger by 0.25 dex;  $\dot{M}$  are averagely smaller by 0.50 dex. There exists a nonlinear relationship between  $L_{\text{Bol}}/L_{\text{Edd}}$  and  $\dot{M}$ ,  $L_{\text{Bol}}/L_{\text{Edd}} \propto \dot{M}^{0.52}$ . For the subsample of 120 RM AGN, the results are similar. With respect to  $\text{FWHM}_{\text{H}\beta}$ ,  $\sigma_{\text{H}\beta}$ -based  $M_{\text{BH}}$  (from the mean spectrum) for the RM subsample are averagely larger by 0.23 dex,  $\dot{M}$  are averagely smaller by 0.43 dex, and  $L_{\text{Bol}}/L_{\text{Edd}} \propto \dot{M}^{0.56}$ . This relation of  $L_{\text{Bol}}/L_{\text{Edd}}$  with  $\dot{M}$  can be derived assuming  $L_{5100}$  is calculated from the standard accretion disk model and  $L_{\text{Bol}}$  is proportional to  $L_{5100}$ .
- Adopting  $L_{\text{Bol}}/L_{\text{Edd}} \propto \dot{M}^{0.5} L_{5100}^{0.25}$ , it means that the converting efficiency  $\eta \propto \dot{M}^{-0.5} L_{5100}^{0.25} \propto (L_{\text{Bol}}/L_{\text{Edd}})^{-1} L_{5100}^{0.5}$ . The nonlinear relation implies that  $\eta$  is anticorrelated with  $\dot{M}$  or  $L_{\text{Bol}}/L_{\text{Edd}}$  (including a relatively weaker dependence on  $L_{5100}$ ), i.e., smaller efficiency with higher dimensionless accretion rate. The efficiency is related to the SMBH spin.
- For the subsample of 4037 SDSS quasars, a strong relation between  $R_{\text{Fe}}$  and  $\dot{M}$  is found:  $R_{\text{Fe}} = -(0.936 \pm 0.006) + (0.600 \pm 0.008) \log \dot{M}$  with the Spearman correlation coefficient  $r_s$  of 0.727. For the subsample of 120 RM AGN, the results are similar with a larger scatter;  $R_{\text{Fe}} = (0.713 \pm 0.047) + (0.532 \pm 0.066) \log \dot{M}$  with  $r_s = 0.423$ . With respect to [O III]  $\lambda 5007$ , the velocity shift  $v_{\text{Fe}}$  has a strong anticorrelation with  $\dot{M}$ , whenever inflow ( $r_s = 0.612$ ) or outflow ( $r_s = -0.419$ ). These strong correlations show that the optical Fe II emission has an intimate connection with the SMBH accretion process.
- Assuming the Fe II clouds fall down from torus with an initial  $v_0 = 0$ , we get the inflow velocity of the optical Fe II  $v_{\text{Fe}}^2 \propto \text{FWHM}_{\text{H}\beta}^2 (1 - M(r) \frac{L}{L_{\text{Edd}}})$ . A smaller  $v$  would be found for AGN with larger  $L_{\text{Bol}}/L_{\text{Edd}}$ , smaller  $\text{FWHM}_{\text{H}\beta}$ . It is qualitatively consistent with the relation of the inflow velocity  $v_{\text{Fe}}$  with  $\text{FWHM}_{\text{H}\beta}$  and  $L_{\text{Bol}}/L_{\text{Edd}}$  or  $\dot{M}$ .
- Assuming a variable  $f$  in  $\text{FWHM}_{\text{H}\beta}$ -based  $M_{\text{BH}}$  from the single-epoch spectrum, we find a strong correlation between  $\log f$  and  $\text{FWHM}_{\text{H}\beta}$ ,  $\log f = (1.719 \pm 0.028) - (0.414 \pm 0.008) \text{FWHM}_{\text{H}\beta}$ . It is flatter than that derived from the mean spectrum for the RM subsample or 17 RM AGN with measured  $\sigma_*$ . However, the relation between  $\log f$  and  $\sigma_{\text{H}\beta}$  is not too strong, suggesting that  $\sigma_{\text{H}\beta}$  doesn't seem dependent much on

the BLR inclination and a constant  $f_\sigma$  is suitable for  $\sigma_{\text{H}\beta}$  as the velocity tracer.

#### ACKNOWLEDGMENTS

We are very grateful to the anonymous referee for her/his instructive comments which significantly improved the content of the paper. This work has been supported by the National Science Foundations of China (Nos. 11973029 and 11873032). This work is supported by the National Key Research and Development Program of China (No. 2017YFA0402703).

#### REFERENCES

- Bentz, M. C., et al. 2013, *ApJ*, 767, 149
- Bian, W. H., & Zhao, Y. H. 2003, *PASJ*, 55, 599
- Bian, W. H., & Zhao, Y. H. 2004, *MNRAS*, 347, 607
- Bian, W. H., et al. 2008, *MNRAS*, 390, 752
- Blandford, R., McKee, C. 1982, *ApJ*, 255, 419
- Boroson, T. A., & Green, R. F., 1992, *ApJS*, 80, 109
- Boroson, T. A. 2002, *ApJ*, 565, 78
- Chelouche, D., & Netzer, H. 2005, *ApJ*, 625, 95
- Collin, S., et al. 2006, *A&A*, 388, 771
- Collin, S., Kawaguchi, T., Peterson, B. M., & Vestergaard, M. 2006, *A&A*, 456, 75
- Dalla Bontà, E., Peterson B. M., Bentz, M. C., et al. 2020, *ApJ*, 903, 112
- Davis, S. W., & Laor, A. 2011, *ApJ*, 728, 98
- Du, P., et al. 2016a, *ApJ*, 818, L14
- Du, P., et al. 2016b, *ApJ*, 825, 126
- Du, P., & Wang, J.-M. 2019, *ApJ*, 886, 42
- Ge, X., Bian, W. H., Jiang, X. L., et al., 2016, *MNRAS*, 462, 966
- Grier, C. J., Martini, P., Watson, L. C., et al. 2013, *ApJ*, 773, 90
- Grier, C. J., Trump, J. R., Shen Y., et al. 2017, *ApJ*, 851, 21
- Ho, L., & Kim, M. 2014, *ApJ*, 789, 17
- Hu, C., Wang, J.-M., Ho, L. C., et al. 2008, *ApJ*, 687, 78
- Hu, C., Wang, J.-M., Ho, L. C., et al. 2012, *ApJ*, 760, 126
- Hu, C., Du, P., Lu, K. X., et al. 2015, *ApJ*, 804, 138
- Hu, C., Li, S. S., Yang, S., et al. 2021, *ApJS*, 253, 20
- Huang, J. et al. 2022, *ApJ*, 895, 114
- Kaspi, S., et al. 2000, *ApJ*, 533, 631
- Kilerci Eser, E., Vestergaard, M., Peterson, B. M., Denney, K. D., Bentz, M. C. 2015, *ApJ*, 801, 8
- Khadka, N., Martínez-Aldama, M. L., Zajaček, M., et al. 2022, *MNRAS*, 513, 1985
- Maithil J., Brotherton, M. S., Shemmer, O., et al. *MNRAS*, in press, (arXiv:2206.11486)
- Marconi, A., Risaliti, G., Gilli, R. et al. 2004, *MNRAS*, 351, 169
- Martínez-Aldama, M. L., Czerny, B., Kawka, D., et al. 2019, 883, 170
- Marziani, P., Sulentic, J. W., Zwitter, T., et al. 2001, *ApJ*, 558, 553
- Mejía-Restrepo, J. E., et al. 2018, *Nature Astronomy*, 2, 63
- McGill, K. L., Woo, J.-H., Treu, T., & Malkan, M. A. 2008, *ApJ*, 673, 703
- Netzer, H., & Trakhtenbrot, B. 2007, *ApJ*, 654, 754
- Netzer, H. 2013, *The Physics and Evolution of Active Galactic Nuclei*
- Onken, C. A., et al. 2004, *ApJ*, 615, 645
- Panda, S. 2022, *Front. Astron. Space Sci.*, 9, 850409
- Peterson, B. M., et al. 2004, *ApJ*, 613, 682
- Shakura, N. I., & Sunyaev, R. A. 1973, *A&A*, 24, 337
- Shen, Y., et al. 2011, *ApJS*, 194, 45
- Shen, Y., & Ho, L. C. 2014, *Nature*, 513, 210
- Shen, Y., Hall, P. B., Horne, K., et al. 2019, *ApJS*, 241, 34
- Sulentic, J. W., Marziani, P., Zamfir, S., & Meadows, Z. A. 2012, *ApJ*, 752, L7
- Urry, C. M., & Padovani, P. 1995, *PASP*, 107, 803
- Wang, J. M., Du, P., Valls-Gabaud, D., Hu, C., Netzer, H., 2013, *Phys. Rev. Lett.*, 110, 081301
- Wang, J. M., Du P., Li Y.-R., Ho L. C., Hu C., Bai J.-M., 2014, *ApJ*, 792, L13
- Woo, J. H., et al. 2015, *ApJ*, 801, 38
- Yu, L. M., Wang, C., Bian, W. H., Zhao, B. X., Ge, X. 2019, *MNRAS*, 488, 1519
- Yu, L. M., Zhao, B. X., Bian W. H., et al. 2020, *MNRAS*, 491, 5881
- Yu, L. M., Bian, W. H., Zhang, X. G., et al. 2020, *ApJ*, 901, 133
- Zhao, B. X., Bian, W. H., Yu, L. M., Wang, C. 2020, *ApSS*, 365, 22